

Influence of Milling Time on the Microstructure and Soft-Magnetic Properties of Nanocrystalline $\text{Fe}_{72}\text{Ni}_8\text{Co}_8\text{Zr}_7\text{B}_4\text{Cu}_1$

K. S. Anand¹ · Sai Rahul Sitaram¹ · Rishav Raj¹ · Anusheela Das¹ · Debottam Goswami² · Jayanta Das¹ 

Received: 13 July 2023 / Accepted: 29 December 2023 / Published online: 7 February 2024
© The Indian Institute of Metals - IIM 2024

Abstract The effect of milling time on the nanostructure, thermal stability, thermomagnetic, and soft-magnetic properties of $\text{Fe}_{72}\text{Ni}_8\text{Co}_8\text{Zr}_7\text{B}_4\text{Cu}_1$ (at.%) upon mechanical alloying up to 72 h have been investigated. X-ray diffraction pattern of the milled powders predominately consists of peaks corresponding to the bcc α -Fe phase. The electron diffraction studies of the 72 h milled powder exhibited an equidistant ring pattern superimposed on a diffuse halo pointing the presence of both nanocrystalline and amorphous phases. After heat treatment, the 60 h milled powder showed the additional diffraction peaks of γ -Ni and bcc-Fe(Cu), corroborating the calorimetric and thermomagnetic analysis. The coercivities (H_C) of powders improved with an increase in mill time. However, the H_C of ball-milled powders was relatively high due to high lattice strain, particle surface roughness, as well as the shape and surface anisotropy of the powder particles.

Keywords Mechanical alloying · Soft magnetic · X-ray diffraction · Magnetometry

1 Introduction

In the recent past, the Fe-based nanocrystalline/glassy alloys have gained widespread attention due to their remarkable

soft-magnetic properties [1–5]. Generally, these soft-magnetic alloys can be described as $\text{FM}_x[\text{M}, \text{ML}, \text{LM}]_{1-x}$, where FM denotes ferromagnetic metals such as Fe, Co, and Ni, M stands for early transition metal, ML denotes metalloid, and LM indicates late transition metal [6]. Some of the well-known Fe-based nanocrystalline/glassy alloys are Fe-Si-B-Nb-Cu [1], Fe-B-Zr-Cu [2], Fe-Co-Zr-B-Cu [3], etc. These alloys possess high saturation magnetization (1.5–1.8 T), tunable Curie temperature (340 K–843 K), and a high permeability ($\sim 10^4$) [1–5]. Besides, Fe-based nanocrystalline/glassy alloys have a wide range of applications, such as in transformer cores, high-frequency antennas, and inductive devices [7, 8].

Generally, techniques such as rapid solidification, gas atomization, or mechanical alloying (MA) are employed to fabricate nanocrystalline/glassy alloys [9]. During MA, the elemental powders are crushed upon milling, causing cold-welding and fracture, leading to chemical homogenization, grain refinement, and formation of metastable phases [9]. MA technique possesses considerable benefits over conventional methods in terms of amorphous alloy processing due to their ability to produce wider compositional ranges and ease of processing towards bulk scale production [9]. Moreover, modern additive manufacturing, fabrication of industrial-scale components, and 3D printing require the precursor to be produced in powder form [10]. On the other hand, the coercivities of milled alloy powders was observed to be relatively high [10].

Although HITPERM alloy ($\text{Fe}_{44}\text{Co}_{44}\text{Zr}_7\text{B}_4\text{Cu}_1$) shows good soft magnetic properties combined with a high Curie temperature [3], the addition of Co in high atomic percentages increases the material cost. However, it was reported that the simultaneous addition of Co and Ni enhances grain refinement [11]. Besides, Ni possesses lower magnetocrystalline anisotropy, which may reduce

✉ Jayanta Das
j.das@metal.iitkgp.ac.in

¹ Department of Metallurgical and Materials Engineering, Indian Institute of Technology Kharagpur, Kharagpur, West Bengal 721302, India

² School of Nano-Science and Technology, Indian Institute of Technology Kharagpur, Kharagpur, West Bengal 721302, India

the effective magnetocrystalline anisotropy of the alloy. Along this direction, few studies have been conducted on Fe–Co–Ni–Zr–B–Cu melt-spun ribbons to investigate their soft-magnetic properties and high-temperature stability [10–12]. However, the melt-spun Fe–Co–Ni–Zr–B–Cu ribbons were reported to have a low thermal stability, thus limiting their applications [10].

In the present work, the mechanical alloying technique was adopted to prepare Fe₇₂Ni₈Co₈Zr₇B₄Cu₁ (at. %) alloy powder whose soft magnetic properties were thoroughly studied. In addition, the evolution of nanostructure and thermal stability of the milled powders were also investigated. Finally, the factors behind the variation of H_C of the milled powders compared to the melt-spun ribbons of similar composition were also identified.

2 Materials and Methods

Fe₇₂Ni₈Co₈Zr₇B₄Cu₁ (at. %) was prepared using a Retsch PM400 MA-type planetary ball-mill using (> 99% pure) elemental powders. Hardened steel vials were loaded with 240 g of balls and 24 g of elemental powder mixture inside an inert Ar glove box (Mbraun GmbH) achieving a 10:1 ball to powder ratio. The milling vials were set to rotate at 250 rpm clockwise and anticlockwise for 15 min each with a pause for 10 min. The as-milled powders were collected after 3 h, 9 h, 18 h, 24 h, 36 h, 60 h, and 72 h. The 60 h milled powder was vacuum-sealed in a quartz tube and heat treated at 773 K for 1 h.

Structural investigations were conducted using an x-ray diffractometer (XRD, Philips PANalytical) and a transmission electron microscope (TEM, FEI Tecnai G2 20). The MAUD package was used for Rietveld refinement [13, 14] to estimate the structural parameters of the constituent phase(s) and crystallite size (d). The simulated diffraction pattern using a Silica standard by considering atomic positions, peak shape and width, scale factors, and background parameters was compared with the experimental diffraction pattern. The parameters were refined using the iterative least square method by minimizing the residual parameters [14]. The particle morphology was investigated using scanning electron microscopy (SEM, JSM-IT300HR-JEOL), attached with an electron dispersive x-ray spectrometer (EDS). Calorimetric studies were performed using differential scanning calorimetry (DSC, PerkinElmer DSC 8000) between 400 and 900 K at a constant heating rate of 10 K/min. The room temperature M - H hysteresis loop measurement up to 15 kOe, and thermomagnetic measurement of heat-treated powder was performed using a vibrating sample magnetometer (VSM, Lakeshore 7407). The field accuracy of the VSM used was 1% of the reading.

The coercivity of the milled powders was measured using an EverCool SQUID VSM (Quantum Design, USA).

3 Results and Discussion

3.1 Structural Analysis

The XRD pattern (Fig. 1a) of the unmilled and milled powders reveals peaks corresponding to bcc- α -Fe and NiZr₂ phases while Fig. 1b represents the zoomed-in patterns of unmilled, 3 h, and 9 h milled powders. The absence of peaks from the elemental Zr, B, and Cu might be due to their significantly lower wt. % than α -Fe in the powder mixture. The hcp-Co peaks were absent after 3 h of milling, and the NiZr₂ peaks were visible in 3 h, 9 h, 18 h, and 24 h milled powders. Moreover, the intensity of the γ -Ni peak drastically reduced after 3 h of milling and was invisible after 9 h of milling. The α -Fe peaks were broadened as milling advanced. Such behavior primarily originates due to the presence of a significant lattice strain or amorphous phase formation during milling.

Greer et al. observed a decrease in $a_{\alpha\text{-Fe}}$ when B atoms diffused into the α -Fe lattice [15]. Similarly, the reduction of $a_{\alpha\text{-Fe}}$ of 3 h (0.2856 ± 0.0001 nm) milled powder compared to that of a pure α -Fe phase ($a_{\alpha\text{-Fe}}^{\text{pure}} = 0.286$ nm) [16] might be due to the diffusion of a significant amount of B atoms into the α -Fe lattice.

A rapid increase in $a_{\alpha\text{-Fe}}$ to 0.2883 ± 0.0001 nm was observed upon 9 h of milling hinting at the diffusion of bigger Zr atoms into the α -Fe lattice. The solid solubility of Ni, Co, and Cu in Fe would not make any significant change in $a_{\alpha\text{-Fe}}$ due to the similarity of atomic size between these atoms [16]. It can be inferred that the solid-state alloying occurred after 9 h of milling since the α -Fe (110) interplanar distance also increased. In addition, the lattice size mismatch of Fe–Co and Fe–Ni is significantly lower than that of Fe–Zr and the elastic energy necessary to form Fe–Ni and Fe–Co solid solution is considerably lower than that of Fe–Zr solid solution [17]. Due a higher elastic energy requirement, higher energy is required for Zr dissolution into the α -Fe lattice compared to other alloying elements [17].

It was noted that the $a_{\alpha\text{-Fe}}$ value suddenly decreased from 0.2883 ± 0.0001 nm at 18 h of milling to 0.2872 ± 0.0001 nm upon 24 h of milling, possibly due to the migration of the solute atoms out of the α -Fe lattice. Such a response of decrease in $a_{\alpha\text{-Fe}}$ after reaching a maximum value in Fe-based nanocrystalline alloys could be attributed to the amorphous phase formation during milling [18]. It should be kept in mind that the NiZr₂ is an intermetallic compound with a fixed stoichiometry; therefore, the possibility of atomic diffusion into the NiZr₂ phase can be ruled out. Therefore, the decrease of $a_{\alpha\text{-Fe}}$ in 24 h milled powder

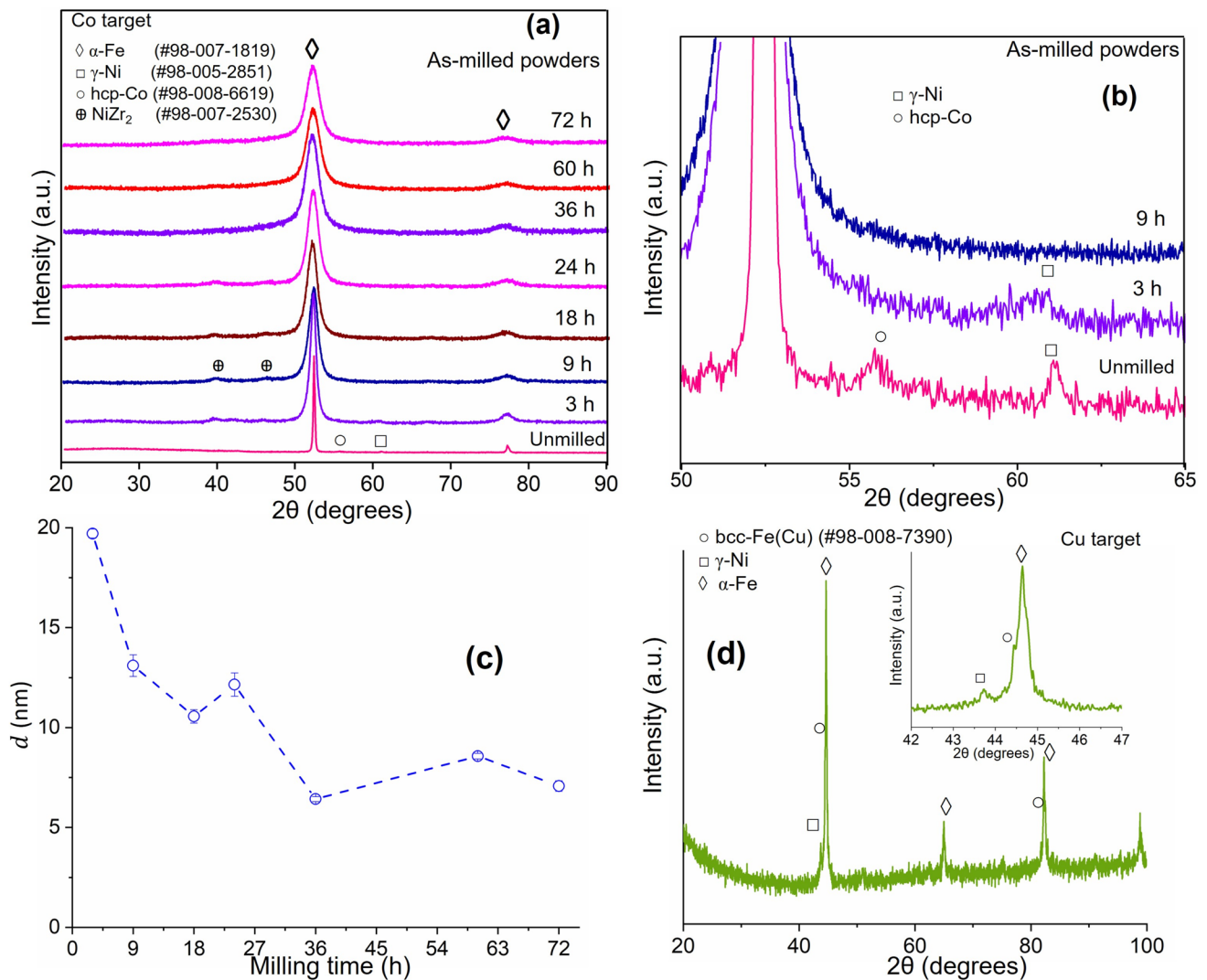


Fig. 1 **a** XRD pattern of the unmillied, 3 h, 9 h, 18 h, 24 h, 36 h, 60 h, 72 h milled powders. **b** Zoomed-in XRD pattern of unmillied, 3 h, and 9 h milled powder **c** variation of d with milling time. **d** XRD

pattern of 60 h milled powder after annealing at 873 K for 1 h. Inset of **d**: zoomed-in version of the same heat-treated powder

was most likely due to the migration of solute atoms from the α -Fe lattice to the newly nucleated glassy phase. The large atomic size mismatch produced by the presence of Zr atom in α -Fe lattice would increase the lattice strain and as a result, the free energy of the crystalline phase would be greater than that of the amorphous phase [19]. Thus, the atomic size mismatch has been found to favor amorphization. Moreover, the d of the samples decreased with an increase in milling time (Fig. 1c), indicating rapid grain refinement during milling. In addition to the aforesaid reason, amorphization can be mechanically-induced as well. It is well-known that the presence of B promotes rapid grain refinement of Fe-based nanocrystalline/glassy alloys during milling, following a process elucidated in refs. [20, 21].

The phase analysis of 60 h as-milled powder solution-annealed at 873 K for 1 h followed by ice-water quenching was conducted to explore the crystallization behavior. After heat-treatment, the XRD pattern consisted of α -Fe, γ -Ni, and a minor bcc-Fe(Cu) peaks, as shown in Fig. 1d, which implied the crystallization of γ -Ni and bcc-Fe(Cu) phase below 873 K. Inset of Fig. 1d represents the zoomed-in version of the same XRD pattern for the range $2\theta=42\text{--}47^\circ$.

The presence of amorphous phase in the milled powders were validated by the SAED pattern of 60 h and 72 h milled powder, as shown in Figs. 2a, b, respectively. The SAED pattern showed a faint equidistant ring pattern and diffused halo ring pattern, confirming both the nanocrystalline bcc phase and the amorphous phase in the milled powders.

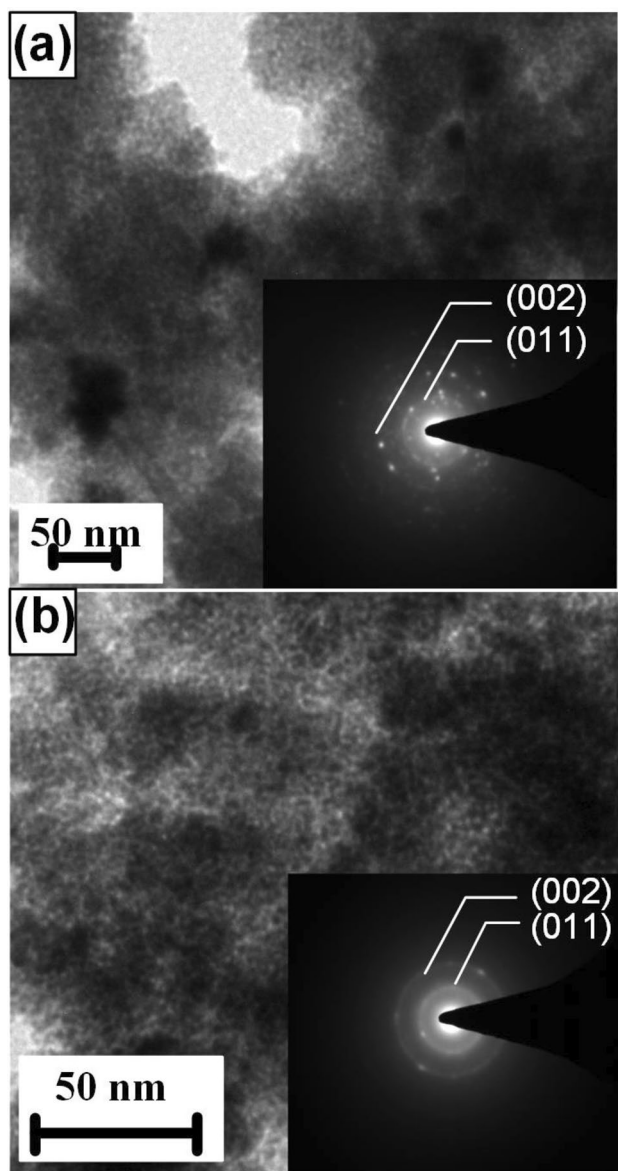


Fig. 2 TEM bright-field image of **a** 60 h and **b** 72 h as-milled powder. Inset: selected area electron diffraction (SAED) pattern of the corresponding microstructure

The RMS lattice strain of 3 h, 9 h, 18 h, 24 h, 36 h, 60 h, and 72 h milled powder was estimated to be $0.4 \pm 0.01\%$, $0.6 \pm 0.03\%$, $0.6 \pm 0.03\%$, $0.8 \pm 0.04\%$, $0.3 \pm 0.04\%$, $0.8 \pm 0.04\%$, and $0.7 \pm 0.01\%$, respectively. A high lattice strain value was generated by the considerable atomic-size mismatch between the constituent elements [21]. Furthermore, high grain boundary fraction due to very small d and mechanical deformation can also give rise to high lattice strain [21].

Figures 3a–g represents the secondary electron (SE) micrographs of unmilled, and variously milled powders, respectively. EDS analysis of 3 h milled powder [inset Fig. 3b] revealed a composition of $\text{Fe}_{77.68}\text{Ni}_{8.37}\text{Co}_{7.64}\text{Zr}_{4.96}\text{Cu}_{1.35}$, (at.%)

which is close to the nominal composition of the alloy without considering Boron.

During milling, those elementary particles trapped between the colliding steel balls were deformed, work-hardened, and fractured [9]. Moreover, the fractured surfaces of these particles cold-welded together [9], increasing the particle size of 3 h of milled powder particles. Furthermore, the particles were flattened and had a non-uniform shape after 3 h of milling (Fig. 3b). Further milling produced slightly elongated particles with considerable surface irregularities (Figs. 3c–g). The 36 h milled powder shows particles in the size range of 3–70 μm which were not altered upon annealing (Figs. 3g, h).

3.2 Calorimetric Studies

Figure 4 depicts the DSC thermogram of 60 h as-milled powder. The endothermic peak during the first heating marks the glass transition event at $T_g \sim 607$ K. Earlier, the XRD pattern showed the crystallization of two phases in Fig. 1d after heat treatment of the milled powder at 873 K. However, no crystallization events were observed in the DSC thermograms, possibly due to the close proximity of the glass transition and the crystallization events. The cooling curve shows no signs of any major events.

3.3 Thermo-Magnetic Studies

Figure 5a shows the M (magnetization) vs H (applied magnetic field) loops of the differently milled powders. The value of M_S was estimated from the M - H plot using the law of approach to saturation, as depicted in Fig. 5b, and expressed as [22]:

$$M = M_S \left(1 - \frac{b}{H^2}\right) \quad (1)$$

where M_S is the saturation magnetization, and b is a constant. The M_S value after 3 h, 9 h, 18 h, 24 h, 60 h, and 72 h of milling was estimated to be 28 emu/g, 104 emu/g, 131 emu/g, 143 emu/g, 126 emu/g, and 139 emu/g, respectively. Due to solid-state alloying, a sudden increase of M_S from 28 emu/g to 104 emu/g was observed after 9 h of milling. The values of coercivity (H_C) (Fig. 5c) were found to decrease with increased milling and the observed values were significantly higher than nanocrystalline alloys prepared by heat treatment of amorphous precursors. Dislocations and the large internal strain generated during milling can be one of the major reasons behind the enhanced H_C values [10]. Upon considering the effect of residual stress, Shen et al. [23] developed an expression for effective anisotropy, K_{eff} and Moreno et al. [24] modified that expression by taking the existence of the amorphous phase into account, as:

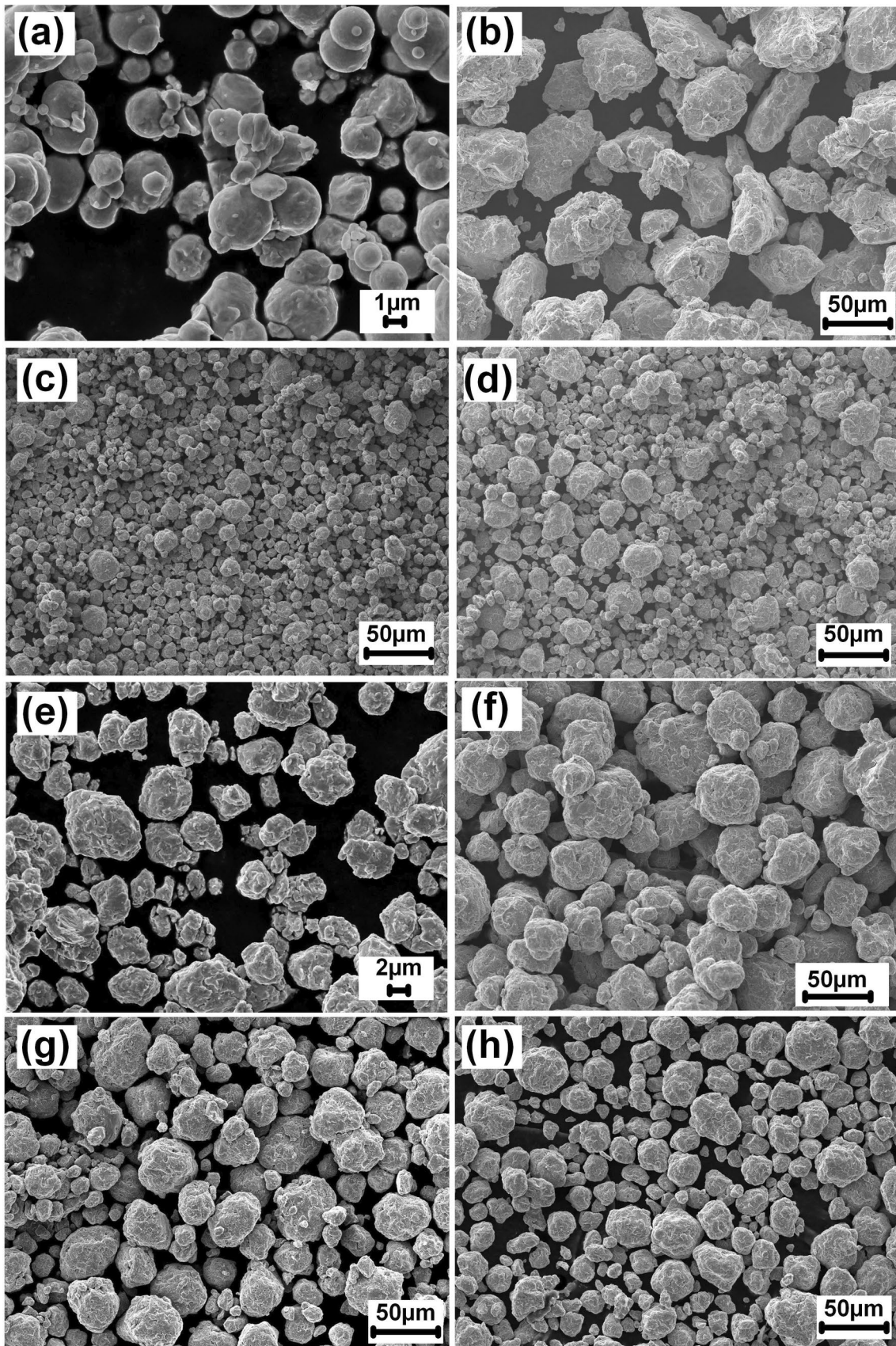


Fig. 3 SEM SE image of **a** un-milled, **b** 3 h, **c** 9 h, **d** 18 h, **e** 24 h, **f** 36 h and **g** 60 h as-milled powders, and **h** annealed at 773 K upon 60 h of milling

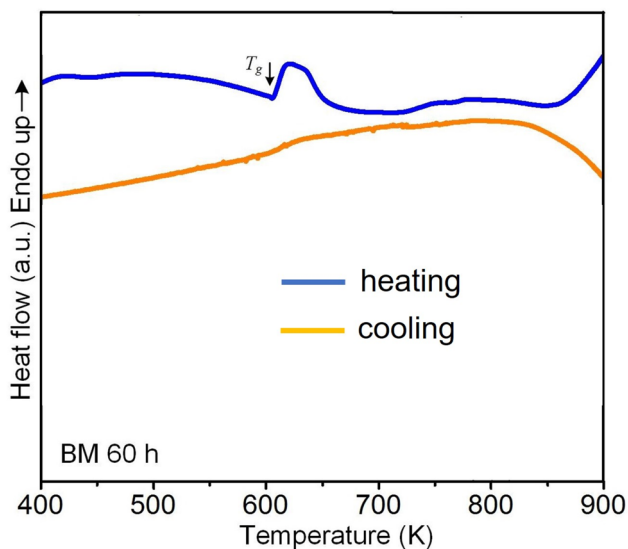


Fig. 4 DSC thermogram of 60 h as-milled powder

$$K_{\text{eff}} = \left(K_{\sigma,\text{ma}}^2 + (K_{\sigma,\text{mi}}^2 + X_{\text{cr}}^2 K_1^2) \frac{d^3 K_{\text{eff}}^{1.5}}{A^{1.5}} \right)^{0.5} \quad (2)$$

where X_{cr} is the crystalline fraction, and A is the exchange stiffness constant. Besides, K_{eff} consists of long-range magneto elastic anisotropy ($K_{\sigma,\text{ma}}$), short-range magnetoelastic anisotropy ($\langle K_{\sigma,\text{mi}} \rangle$), and magnetocrystalline anisotropy ($\langle K_1 \rangle$). Moreover, K_{eff} can also be expressed as [25]:

$$K_{\text{eff}} = \frac{H_C M_S}{P_C} \quad (3)$$

where the value of the constant, P_C lies between 0.13 and 0.64. During milling, $\langle K_1 \rangle$ gets suppressed due to grain refinement, which in turn decreases K_{eff} and as a result the value of H_C decreases following Eq. 3. Moreover, the increase of amorphous phase fraction, i.e., decrease in X_{cr} , can also contribute to the reduction of H_C .

The larger shape anisotropy created by high surface irregularities can also yield a large H_C value [26, 27]. As demonstrated in Fig. 6, the milled powder particles have a significant amount of surface irregularities. The elongated morphology of the milled particles (see Fig. 3) can also be a source of shape anisotropy. Stoner and Wohlfarth proposed that the coercivity of randomly oriented elongated particles as [28]:

$$H_C = 0.479(N_t - N_o)M_S \quad (4)$$

where, N_t and N_o is the demagnetization factor for the long and short axis, respectively. Assuming that the 72 h milled powder particles to be prolate or oblate ellipse whose

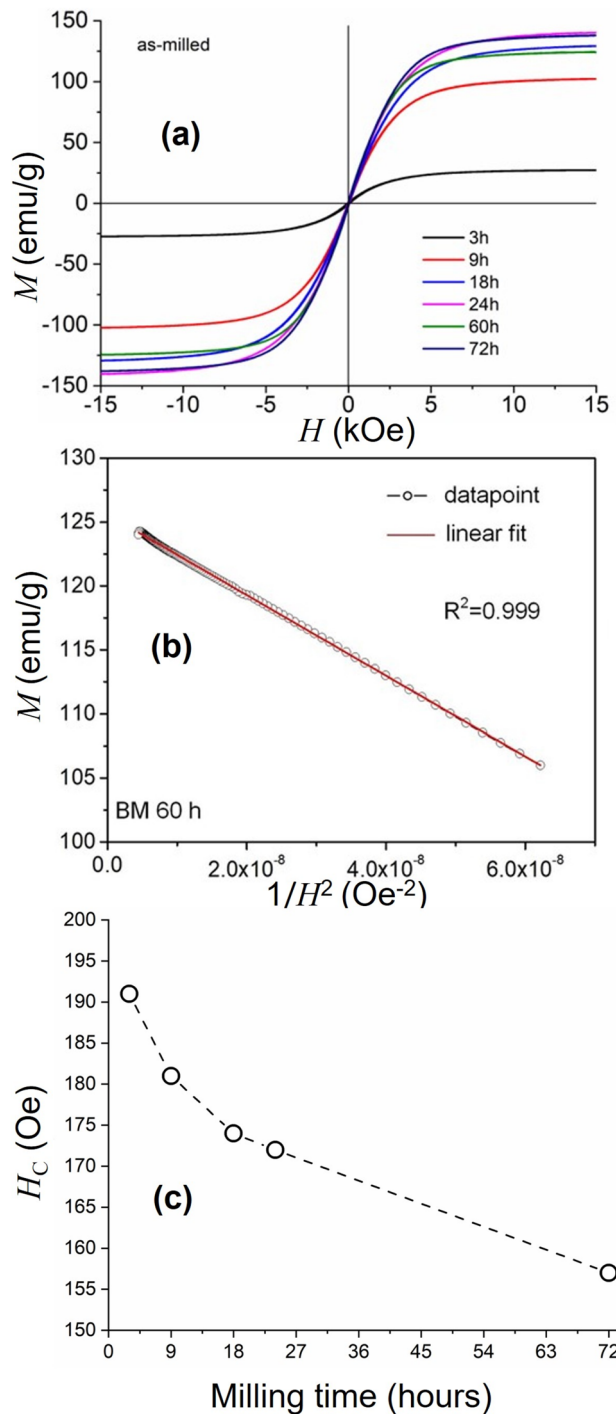


Fig. 5 a M - H loop of differently milled powders upto 15 kOe. b Linear fitting of 60 h milled powder according to law of approach to saturation. c Variation of H_C of the as-milled powders with milling time

long axis is 1.2 times the short axis, then the value of $N_o \approx 0.3$ [28], hence $N_t = 1 - (2 \times 0.3) = 0.4$ [29]. The M_S value for 72 h milled powder was converted to 1.36 T using the simple rule of mixtures. Using Eq. 4, the value of H_C was

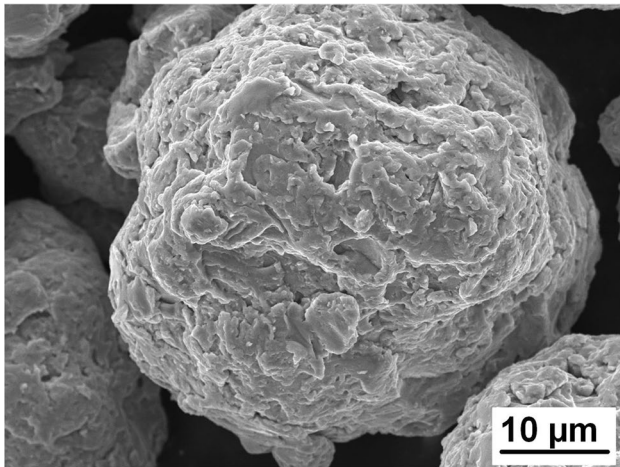


Fig. 6 SEM SE image of 60 h as-milled powder at a higher magnification

estimated to be 651 Oe, which is much greater than the observed value. Such a low H_C was observed, as the milled particles were mostly larger than a single domain size, with probably a few single domain particles existing in the milled powders.

The high surface anisotropy also plays a critical role in the enhanced H_C of milled powders. In very small-sized particles, (Fig. 7), the surface to volume ratio is larger, meaning a significant fraction of atoms are surface atoms [30]. In such circumstances, a site-specific surface anisotropy arises due to the symmetry breakage of these surface atoms [27]. Furthermore, the broken bonds result in surface spin disorder and frustration leading to an inverse relation of surface anisotropy to the particle sizes.

The remanence (M_R) of the milled powders after 3 h, 9 h, 18 h, 24 h, 60 h, and 72 h of milling was estimated to

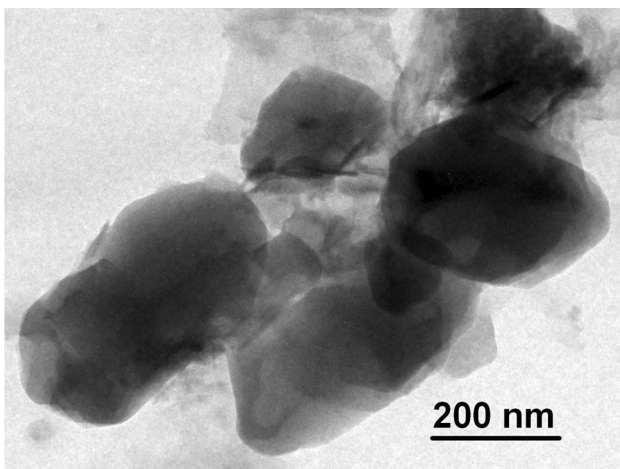


Fig. 7 TEM bright-field image of 72 h as-milled powder

be 0.76 emu/g, 1.86 emu/g, 1.59 emu/g, 2.18 emu/g, 1.30 emu/g, and 1.22 emu/g respectively. The squareness ratio ($\frac{M_R}{M_S}$) of the powders were 0.027, 0.017, 0.012, 0.015, 0.010, and 0.009, respectively. The squareness ratio is significantly lower than the theoretical value predicted for isotropic (0.5) or cubic Stoner–Wohlfarth particle (0.83) [31]. Such a low $\frac{M_R}{M_S}$ value was also ascribed to the demagnetization effects. The relationship between the applied field (H_a) and internal field (H_i) can be expressed as [31]:

$$H_i = H_a - N_d \langle M \rangle \quad (5)$$

where $\langle M \rangle$ is the average magnetization at a given field and N_d is the demagnetizing factor. Furthermore, $N_d \langle M \rangle \geq H_a$ when H_a is very close to zero, the local demagnetizing field is just strong enough to nucleate new domains and enable the displacement of those newly created domains [27]. As a result, $\frac{M_R}{M_S}$ ratio decreases to < 0.5 [27].

Figure 8 illustrates the magnetic moment versus temperature plot of 60 h milled and annealed powder. A ferromagnetic to paramagnetic transition of γ -Ni phase is observed at ~ 600 K, prior to which, the moment gradually increases. Due to extended milling, few particles may have attained sizes below a critical value, which causes an increased moment due to a ferromagnetic to super-paramagnetic transition [32]. After the transition of γ -Ni, the moment increases again indicating the bcc-Fe(Cu) phase formation. The moment drastically decreases beyond 950 K due to the ferromagnetic to the paramagnetic transition of α -Fe. Still, the alloy showed a slight moment at

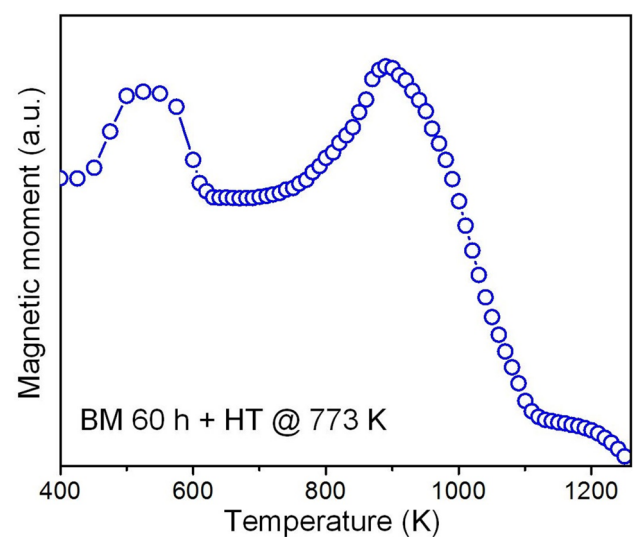


Fig. 8 Thermomagnetic plot of 60 h milled powder annealed at 773 K for 1 h

the paramagnetic regime of α -Fe due to the presence of the bcc-Fe(Cu) phase, which reduced to zero > 1200 K.

4 Conclusions

The structural, calorimetric, soft magnetic, and thermomagnetic properties of differently milled nanocrystalline $\text{Fe}_{72}\text{Ni}_8\text{Co}_8\text{Zr}_7\text{B}_4\text{Cu}_1$ (at. %) powders have been investigated. The following conclusions have been drawn:

- The XRD analysis of the as-milled powders revealed the presence of α -Fe peaks. The crystallite size of the milled powders decreased from 20 to 7 nm with an increase in ball milling duration. The SAED pattern revealed the presence of nanocrystalline and amorphous phases in 60 h and 72 h as-milled powder. While the first heating DSC curve showed the presence of a glass transition event, the second heating curve detected two exothermic events due to the formation of γ -Ni and bcc-Fe(Cu) phase.
- Due to factors such as the grain refinement and reduction of K_{eff} the H_C value reduced with milling time. The relatively higher H_C of the differently milled powders compared to that of melt-spun ribbons might be due to a variety of factors such as large lattice strain, particle surface roughness, shape anisotropy, and surface anisotropy.

Acknowledgements The authors thank Mr. S. Maity and Mr. R. Bosu of the Central Research Facility, IIT Kharagpur for technical assistance.

Funding This work was supported by Sponsored Research and Industrial Consultancy (SRIC), IIT Kharagpur through SGBSI project.

References

1. Yoshizawa Y, Oguma S, and Yamaguchi K, *J Appl Phys* **64** (1988) 6044.
2. Suzuki K, Kataoka N, Inoue A, Makino A, and Masumoto T, *Mater Trans JIM* **31** (1990) 743.
3. Willard M A, Laughlin D E, McHenry M E, Thoma D, Sickafus K, Cross J, and Harris V G, *J Appl Phys* **84** (1998) 6773.
4. Iwanabe H, Lu B, McHenry M E, and Laughlin D E, *J Appl Phys* **85** (1999) 4424.

5. Wei R, Tao J, Sun H, Chen C, Sen G W, and Li F S, *Mater Lett* **197** (2017) 87.
6. Suzuki K, *Mat Sci Forum* **321** (1999) 521.
7. Herzer G, *Acta Mater* **61** (2013) 718.
8. Nowroozi M A, and Shokrollahi H, *Adv Powder Technol* **24** (2013) 1100.
9. Suryanarayana C, *Prog Mater Sci* **46** (2001) 1.
10. Thomas S V, Willard M A, Martone A, Heben M J, Solomon V, Welton A, Boolchand P, Ewing R C, and Wang C, *Phys Status Solidi A* **217** (2020) 1900680.
11. Knipling K E, Daniil M, and Willard M A, *J Appl Phys* **117** (2015) 172611.
12. Fan X, Tang Y, Shi Z, Jiang M, and Shen B, *AIP Adv* **7** (2017) 056107.
13. Lutterotti L, MAUD, CPD Newsletter (IUCr) No. 24, December (2000)
14. Young R A, Introduction to the rietveld method. in *The Rietveld Method*, (ed) Young R A, Oxford University Press, Oxford (1993), pp 1–38.
15. Greer A L, *Acta Metall* **30** (1), (1982) 171.
16. Liu Y J, and Chang I T H, *Acta Mater* **50** (2002) 2747.
17. de Boer F R, Boom R, Mattens W C M, Miedema A R, and Niesen A K, *Cohesion in Metals*, Elsevier Sci. Publishers B.V, Holland (1988).
18. Sharma S, and Suryanarayana C, *J Appl Phys* **102** (2007) 083544
19. Ogino Y, Murayama S, and Yamazaki Y, *J Less-Common Met* **168** (1991) 221.
20. Izadi S, Janghorban K, Akbari G H, Ghaffari M, and Salahinejad E, *J Alloys Compd* **493** (2010) 645.
21. Taghvaei A H, Stoica M, Khoshkhou M S, Thomas J, Vaughan G, Janghorban K, and Eckert J, *Mater Chem Phys* **134** (2012) 1214.
22. Chikazumi S, *Physics of Magnetism*, Wiley, New York (1964).
23. Shen T D, Schwarz R B, and Thompson J D, *Phys Rev B* **72** (2005) 014431
24. Moreno L, Blázquez J, Ipus J, and Conde A, *J Alloys Compd* **585** (2014) 485.
25. Herzer G, *IEEE Trans Magn* **26** (1990) 1397.
26. Kronmüller H, and Gröger B, *J Phys (Fr)* **42** (1981) 1285.
27. Zeng Q, Baker I, McCreary V, and Yan Z, *J Magn Magn Mater* **318** (2007) 28.
28. Stoner E, and Wohlfarth E, *Trans R Soc A* **240** (1953) 599.
29. Osborn J A, *Phys Rev* **67** (1945) 351.
30. Bødker F, Mørup S, and Linderoth S, *Phys Rev Lett* **72** (1994) 282.
31. Morrish A H, *The Physical Principles of Magnetism*, Wiley, New York (1965).
32. Hopkinson O J, *Proc R Soc Lond* **48** (1890) 1.

Publisher's Note Springer Nature remains neutral with regard to jurisdictional claims in published maps and institutional affiliations.

Springer Nature or its licensor (e.g. a society or other partner) holds exclusive rights to this article under a publishing agreement with the author(s) or other rightsholder(s); author self-archiving of the accepted manuscript version of this article is solely governed by the terms of such publishing agreement and applicable law.